Original research

# PVP-assisted laser ablation growth of Ag nanocubes anchored on reduced graphene oxide (rGO) for efficient photocatalytic $CO_2$ reduction

Rui Zhou[a],[*],[1], Yuanchao Yin[a],[1], Deng Long[b], Jingqin Cui[b], Huangping Yan[a], Wanshan Liu[a], Jia Hong Pan[c],[**]

[a] School of Aerospace Engineering, Xiamen University, Xiamen, Fujian Province, 361102, China
[b] Pen-Tung Sah Institute of Micro-Nano Science and Technology, Xiamen University, Xiamen, Fujian Province, 361005, China
[c] MOE Key Laboratory of Resources and Environmental Systems Optimization, College of Environmental Science and Engineering, North China Electric Power University, Beijing, 102206, China

## ABSTRACT

Metallic nanoparticles loaded graphene nanocomposites have been widely studied for various scientific and technological applications. In this study, a facile method was reported to realize a straightforward growth of shape and size-controllable of metallic nanoparticles, and the subsequent hybridization with graphene in solution by strategically coupling wet-chemical route and laser ablation. By mixing graphene oxide (GO) with a tunable concentration level of polyvinylpyrrolidone (PVP) in aqueous solution, Ag nanocubes with a face-centered cubic crystal structure were generated by pulsed laser ablation and then mounted on GO nanosheets with the assistance of PVP. The preferential adsorption of PVP to Ag (100) crystal face led to the production of Ag nanocubes with exposed (100) facet. The result showed that the morphological yield of spherical particles decreased with the increase in PVP concentration. X-ray diffraction (XRD) and UV–visible spectroscopy analyses confirmed that GO was partially reduced. In the reduction of $CO_2$ gas, the photocatalytic conversion rate could achieve $133.1\ \mu mol\ g^{-1}\ h^{-1}$ in 6 hrs for cubic Ag-loaded reduced GO composites.

## 1. Introduction

The issue of $CO_2$ emission has been a major concern in the world. How to effectively convert $CO_2$ into chemicals and fuels has been the focus of research. The carbon in $CO_2$ is in the highest oxidation state and can be reduced to various carbon compounds, such as CO, methane and higher hydrocarbons in gas phase, or methanol ($CH_3OH$) and formic acid (HCOOH) in liquid phase [1]. Catalytic reduction by solar active catalysts serves as one of the effective methods for the reduction of carbon dioxide [2,3]. As a typically photoactive metal material, Ag nanoparticles have been widely used as a photocatalyst based on the surface plasmon effect or as a co-catalyst for effective photogenerated charge carrier separation, both of which have demonstrated to be beneficial for photocatalytic reduction of $CO_2$ [4]. For example, Zhou et al. [5] successfully reduced $CO_2$ to CO by electrochemical reduction using polycrystalline Ag. Asi M. A. et al. [6] synthesized Ag/AgBr/carbon nanotubes for photocatalytic reduction of $CO_2$ to methane, CO, methanol, etc. Various types of Ag nanostructures, such as sphere, rod,

wires and cube, have been chemically synthesized [7], among which the cubic Ag nanoparticles able to deliver a stronger Raman signal than the nanospheres and nanowires are of particulate interest. The remarkable enhancement is mainly ascribed to more edges of cubic structure, resulting in a higher intensity of local electromagnetic fields [8].

Wet-chemical method has been usually used to fabricate cubic Ag nanoparticles, but unfortunately it is easy to bring in complicated procedure and inevitable by-products. In contrast, laser ablation is a unique green manufacturing method for nanoparticle synthesis [9–11]. Upon laser irradiation on the metal surface with the assistance of surfactant directed stabilization, it is possible to design the structure of metallic nanoparticle in different shapes. In addition, laser ablation produces less by-products, which was firstly demonstrated by Fojtik and Henglein [12]. Therefore, the quality of nanoparticles studied could not be affected by these uncontrolled substances. During the selection of surfactants that can adjust the structure of Ag nanoparticle, PVP is deemed as one of the most popular surfactants due to its steric

hindrance effect and strong adsorption to Ag nanoparticle, which contributes to the fabrication of Ag nanoparticles in different shapes. Meanwhile, PVP molecules interact with the substances generated by laser ablation of metal surface to prevent them from agglomeration, leading to the creation of stable nanoparticles in a controllable particle size and shape [13].

Graphene is a multifunctional 2D materials showing diverse fantastic properties, including large surface area, high electrical conductivity, extremely high electron mobility, excellent thermal conductivity etc. Besides, These similar remarkable characteristics also enable easily prepared graphene oxide (GO) to be used in different fields as a typical 2D material with high oxygen functionalities and large specific surface area [14]. In the photocatalytic reaction, it is proved that GO or reduced GO (rGO) can promote the separation process of photogenerated electrons and holes, leading to higher photocatalytic activity [15]. Graphene-based materials can be used as scaffolds for the deposition of Ag nanoparticles. Under light irradiation, free electron-hole pairs can be generated due to surface plasmon effect of Ag. Typically, free electrons can transfer to graphene-based nanosheets (e.g. graphene and rGO) that are highly conductive, by which holes and electrons can be effectively separated.

In this paper, pulsed laser ablation has been developed to synthesize Ag nanocubes loaded rGO composite from a PVP-containing GO solution. By adjusting the concentration of PVP, the size and morphology of the Ag nanocubes deposited on rGO nanosheets can be tuned, and their efficiencies in photocatalytic reduction of $CO_2$ can be optimized.

## 2. Experimental

### 2.1. Materials

High-purity (99.99%) Ag plates (with a thickness of 0.6 mm) were purchased from Guoyu Electronic Material Factory (GY056) and used as the targeted metal substrates. Before use, Ag plates were sufficiently washed with DI water and ethanol. PVP K30 (molecular weight ~40000) were purchased from Sigma-Aldrich Corporation. GO, prepared by chemical intercalation-thermal expansion method, was purchased from Shanxi Institute of Coal Chemistry. The particle size of GO nanosheet was distributed from 0.1 to 3.0 μm.

### 2.2. Fabrication of Ag loaded graphene nanocomposites

The Ag plate (25 mm × 25 mm) was fixed at the bottom of a glass vessel. Homogeneous PVP aqueous solution with a concentration ranging from 4.5 to 180.2 mM) with well dispersed GO upon ultrasonic treatment for 1 hr was employed to create a liquid environment for the generation of rGO-Ag nanoparticle (rGO-AgNP) hybrid materials. The height difference between water/air interface and the targeted plate was about 2 mm. A pulsed laser of the wavelength 1064 nm and pulse width ~100 ns was used to irradiate the Ag plate at a repetition frequency 20 kHz and constant power 24 W. The ablation area on the sample surface was 5 mm × 5 mm for 20 mins' ablation. Here, a control group is set as rGO-Ag-1, where the Ag plate was ablated only in GO solution free of surfactant. In contrast, the desired composite material named rGO-Ag-2 was prepared by filling the solution with an optimized level of PVP concentration (180.2 mM). The schematic of laser ablation on Ag substrate in GO aqueous solution is shown in Fig. 1.

After the laser ablation, the nanocomposite dispersions were washed with ethanol and recovered by centrifugation at 15000 rpm. The sediment was dispersed in ethanol and sonicated for 10 mins to repeat the wash. After five-cycle washing, the samples were collected and dried under vacuum at room temperature.

### 2.3. Photocatalytic reduction of $CO_2$

The process of photocatalysis for $CO_2$ reduction was conducted at airtight stainless photocatalytic reaction kettle (Shanghai Guigo Industrial Co., Ltd, volume, ~400 mL), at a pressure of 0.2 MPa filled with $CO_2$ and temperature of 318.5 K. Thus, 50 mL of deionized water was stored at the bottom of the chamber as hydrogen source by continuously stirring during the whole process. In the step of lightening, 300 W Xenon Lamp (Beijing Zolix) worked for 6 hrs. Then the final product was extracted for 50 μL and injected to the Flame Ionization Detector (FID) of gas chromatography (GC 9790 Fu Li Co., Ltd) for the composition analysis of the gas mixture. The yield of CO directly reflects the $CO_2$ reduction rate, which can clearly indicate the photocatalytic performance of the as-prepared samples. Herein, Ag nanoparticles and graphene oxide were set as pure substance control groups. The composite rGO-Ag-1 was Ag nanospheres combined with reduced graphene oxide free of surfactant stabilization, and rGO-Ag-2 was Ag nanocubes with reduced graphene oxide by the surfactant directed fabrication in an optimized level of PVP concentration. Each group of samples was measured three times after 6 hrs' reaction period. Finally, the average value was used to evaluate the photocatalytic performance of $CO_2$ reduction for as-prepared samples. CO collected by a strip is obtained by photocatalytic reduction under the illumination wavelength 310–700 nm, 500 μL of which could be extracted by a syringe. The percentage of CO could be detected by gas chromatography to calculate the reaction rate of photocatalytic reduction of $CO_2$. Herein, the pressure is set as 0.2 MPa, the density of $CO_2$ is 3.6 Kg/m³, the volume of the gas used is 400 mL, and the mass of $CO_2$ is 1.44 g.

### 2.4. Material characterization

Analysis of particle size and morphology is performed by scanning electron microscopy (ZEISS SUPRA 55) to obtain size distribution of particles. GO-Ag nanocomposites obtained were deposited on silicon wafer, which was further dried at room temperature overnight. Further structural analysis of Ag cubic particle is performed by transmission electron microscope (F30). The crystal structure was analyzed by X-ray diffraction (40 kV, 80 mA, Cu Ka) with a 2θ step size of 0.02. The UV–visible spectroscopy (UV 2600 220V CH) was employed to investigate absorption spectra of the synthesized samples at a wavelength rang of 200–700 nm.

## 3. Results and discussion

### 3.1. Structure of Ag nanoparticles

The concentration of PVP plays a vital role in tuning the morphology of Ag nanoparticles. Fig. 2 shows various morphologies of Ag nanoparticles including spheres, cubes, and a few types of triangles under different concentrations of PVP. Spherical Ag nanoparticles in the size of 10–40 nm were mainly produced while the PVP concentration was lower than 18.0 mM, as observed in Fig. 2a and b. When the PVP concentration increases up to around 45 mM, Fig. 2c shows that cubic structure appears due to the assembly of PVP molecules. In Fig. 2d–f, a large number of cubic structures are generated along with further increasing the concentration level of PVP. It may be attributed to the tightly dense coverage of the Ag (100) plane with high concentration of PVP molecules, resulting in a significant flux of Ag atoms preferably moving to the Ag (111) plane. Finally, (100)-faceted nanocubes are dominantly formed by the anisotropic growth effect.

### 3.2. Ag loaded graphene oxide

SEM and TEM images for the intercalated structure of cubic Ag nanoparticles and GO sheets for rGO-Ag-2 are summarized in Fig. 3. Cubic Ag nanoparticles are almost monodispersed and evenly distributed on GO nanosheet, which further avoids the agglomeration of ultrafine Ag nanoparticles. Combined with SAED analysis in Fig. 3d, the *d-spacing* of the as-prepared composite is evaluated as 0.24 nm by
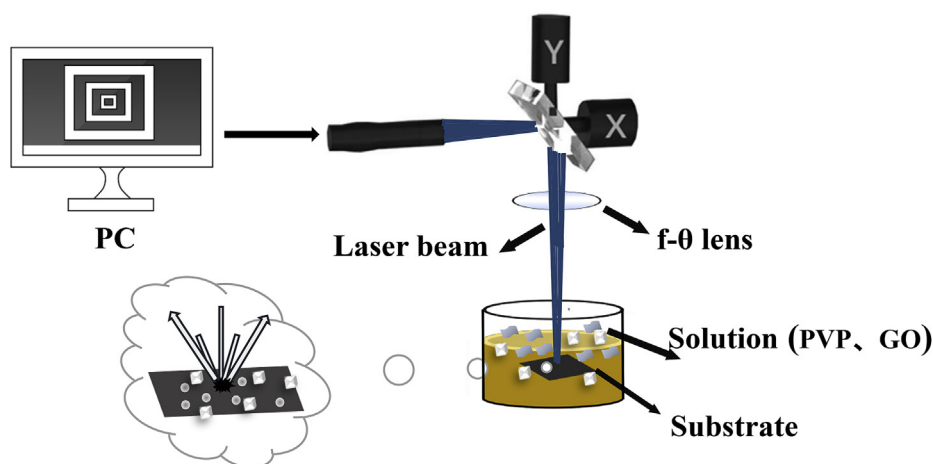
**Fig. 1.** Schematic diagram of fabricating Ag-loaded graphene-based composite by laser ablation.

performing TEM, which is attributed to the (111) diffractive plane of Ag. Meanwhile, the SAED pattern of rGO-Ag-2 nanocomposite shows the characteristic rings of the fcc Ag (111), (200), (220) and (311) planes caused by the high crystalline of the Ag-loaded GO nanocomposites [16]. The adsorption of PVP on the (100) crystal plane of Ag inhibits the growth of the surface, leading to the acceleration of the growth of other crystal faces to form a cubic structure. The rGO sheet acts as a stabilizer to prevent the aggregation of Ag nanoparticles, so that the obtained cubic Ag nanoparticles are riveted on rGO sheet. The intercalation between graphene-based sheets and Ag nanoparticles facilitates the smoother transmission of photogenerated electrons by increasing the number of surface active sites based on the uniformly distributed Ag nanoparticles on the support, which could be beneficial for the photocatalytic reduction of $CO_2$ [17].

Fig. 4 shows the XRD patterns of Ag, GO and rGO-Ag-2. The peak of GO at 10° in the curve (c) disappeared in the sample of rGO-Ag-2, and the peaks at 26.6° and 54.2° are derived from the (002) and (004) planes of graphene-based nanosheet, respectively, which is attributed to the rGO and the graphite structure in the supporting materials of as-

prepared composite [18]. The peaks at 38.2°, 44.3°, 64.5°, 77.7° and 81.6° are assigned to the Ag crystals, corresponding to the (111), (200), (220), (311) and (222) crystal planes of Ag (JCPDS index No. 41-1402), respectively, which indicates the face-centered cubic structure of Ag crystals. In the curve (b), the peak of the (111) crystal plane is significantly enhanced compared to curve (a), indicating that the selective adsorption of the PVP molecules to the Ag (100) crystal plane. Therefore, it enhances the growth of (111) crystal plane. Besides, the (111) crystal plane in curve (d) continues to increase, indicating that the addition of the graphene-based material further contributes to the dispersion of the Ag nanoparticles. A possible explanation is that rGO might act as a stable dispersant for the uniform anchor of laser ablated Ag nanoparticles, which significantly prevents the aggregation of Ag nanoparticles [19]. Previous research has shown that graphene can act as a stabilizer to assist the formation of stable metallic nanoparticle colloids [20]. The stronger and narrower peak width of Ag peaks in XRD pattern indicate the higher crystalline structure in the cubic Ag nanoparticles under the collective effect of PVP and rGO.
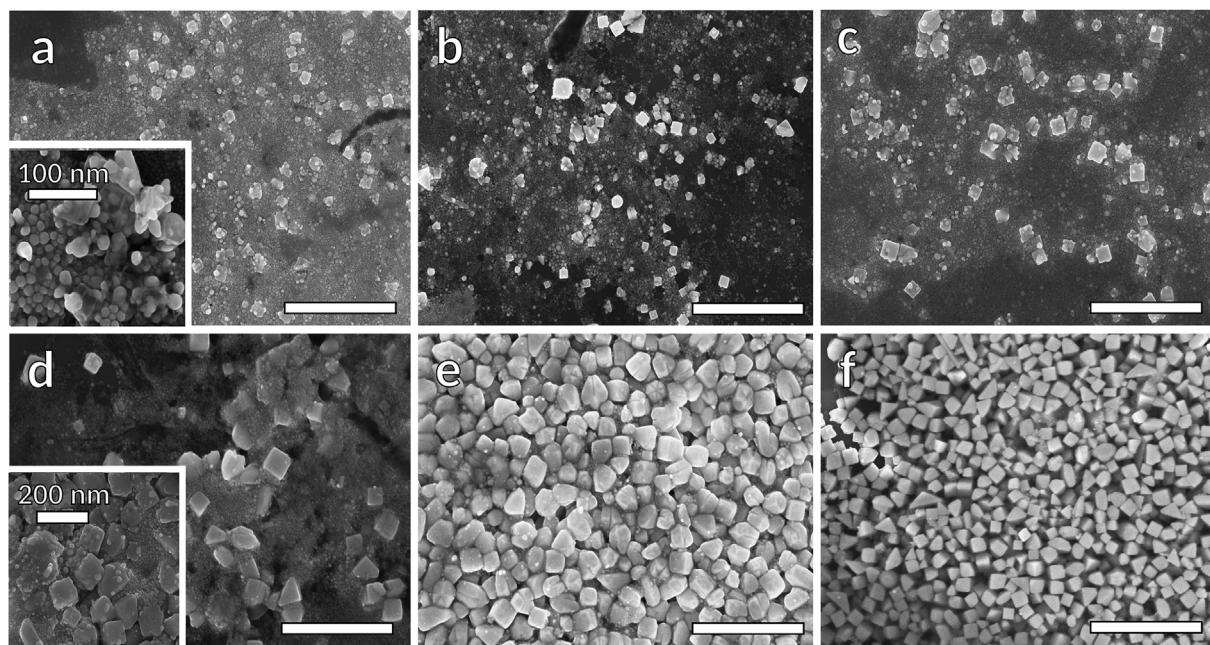


**Fig. 2.** Ag nanoparticles generated by laser ablation at different PVP concentrations. (a) 4.5 mM; (b) 9.0 mM; (c)18.0 mM; (d) 45.0 mM; (e) 90.1 mM; (f) 180.2 mM. All scale bars are 1 μm.
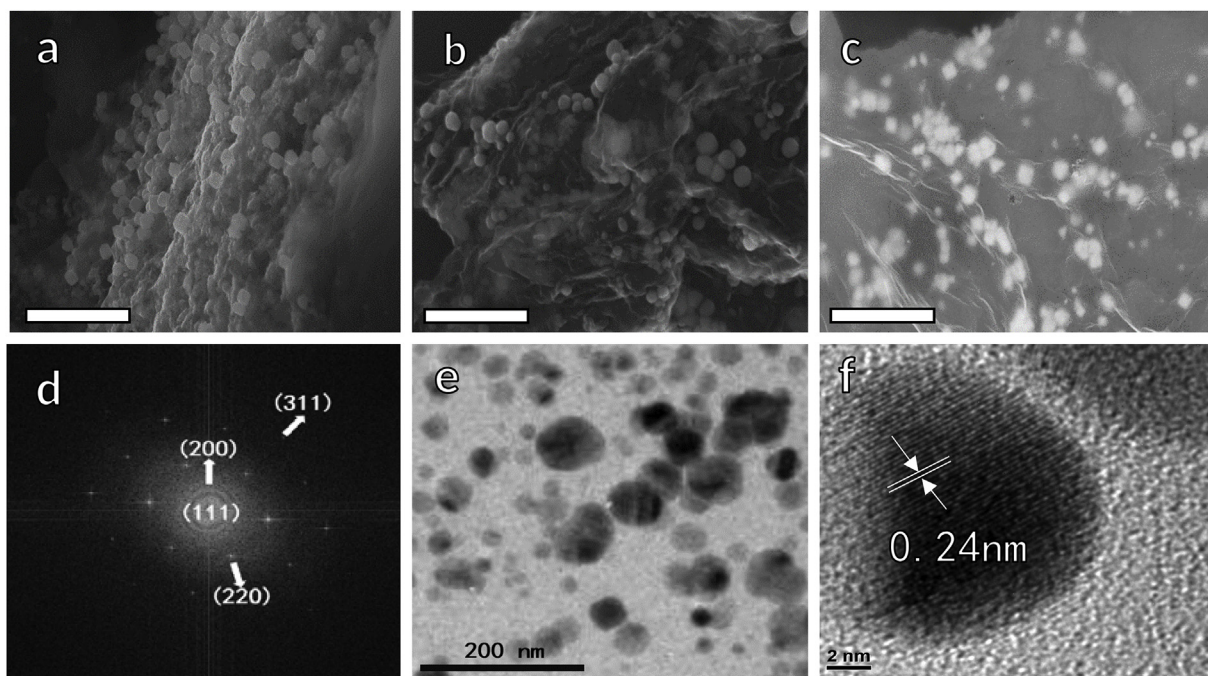
**Fig. 3.** (a–c) SEM images of cubic Ag nanoparticles loaded on rGO for rGO-Ag-2. Scale bars are 200 nm; and (d–f) TEM images of loaded cubic Ag nanoparticles.
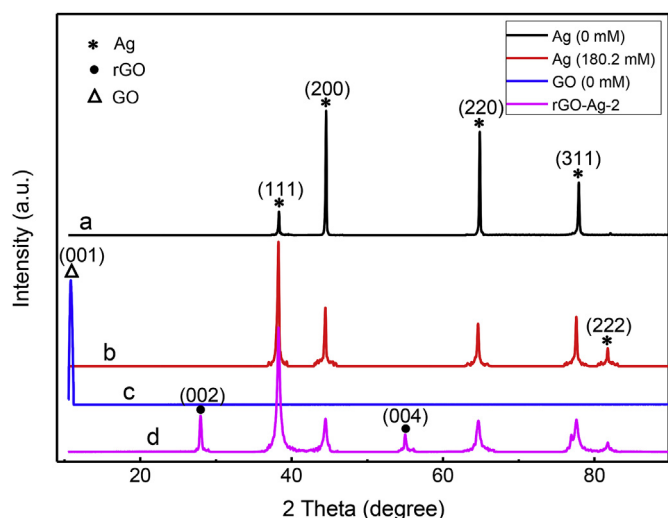


**Fig. 4.** XRD patterns of (a) Ag nanoparticles without PVP; (b) Ag nanoparticles synthesized with PVP (180.2 mM); (c) original GO; and (d) rGO-Ag-2 nanocomposites synthesized with PVP (180.2 mM).

### 3.3. UV–visible absorption

Fig. 5a shows UV–visible absorbance spectra of Ag nanoparticles with different structures under the influence of different concentrations of PVP. The UV–visible absorption peaks of the three lower concentrations are consistently located at about 402 nm, which is a typical plasmon resonance absorption peak for spherical Ag nanoparticle [21]. The absorption peaks of the three higher concentrations have been found to be red-shifted at around 412 nm, which indicates that the edges of the nanoparticle gradually increases from the sphere to the cube [22]. And the increase in the size of the Ag nanoparticles also results in the red shift [23]. In addition, the formation of anisotropic Ag nanocrystals contributes to the asymmetry of UV–visible spectra of the three higher concentrations. After loading Ag nanoparticles on the graphene-based support, a sharp and prominent absorption peak of as-prepared GO approximately at the wavelength of 230 nm is related to π-

π* transitions of aromatic C–C bonds, as shown in Fig. 5b, while n-π* transitions of C=O bonds is corresponding to the shoulder at 300 nm [24]. The absorption peak of as-prepared rGO-Ag-2 composite shifts to 250 nm, corresponding to the peak of reduced GO [22]. The weak peak at 300 nm belongs to the remaining GO in the solution, indicating that laser ablation could partially reduce the graphene oxide during the fabrication [25]. This is corresponding to the XRD pattern where the peaks of rGO at 26.6° and 54.2° could be observed in Fig. 4. Besides, in the composite material rGO-Ag-2, the absorption peak of the Ag nanocubes was blue-shifted due to the reduced particle size of the Ag nanocubes. The possible reason is that a longer ablation duration is conducted for the composite, leading to the decrease of average nanoparticle size by re-ablation of the existing nanoparticles [26]. In this case, the intensity of irradiated laser on the surface of the Ag substrate is partially absorbed by GO, leading to a decreased size of formed nanoparticles [27].

### 3.4. Photocatalytic reduction of $CO_2$

The photocatalytic activity for rGO-AgNP nanocomposites was evaluated by the reduction of $CO_2$. As reported previously, CO production in a high selectivity can be achieved over Ag surface [28]. Therefore, the yield of CO is represented by the reaction rate of $CO_2$. Fig. 6 summarizes the photocatalytic activities of rGO-Ag-1 and rGO-Ag-2 in $CO_2$ reduction, compared to the pure GO and Ag nanoparticles with 43.6 and 65.4 $\mu mol\,g^{-1}\,h^{-1}$, respectively. While the reaction rate of rGO-Ag-1 (with spherical Ag nanoparticles) and rGO-Ag-2 (with cubic Ag nanoparticles) are obviously 2–3 times higher than those control samples, achieving 120.1 and 133.1 $\mu mol\,g^{-1}\,h^{-1}$, respectively. It shows that there is a significant enhancement of photocatalytic reduction capability after the collaborative effect of the Ag nanoparticles and GO. Also, the photocatalytic performance could be significantly affected by the structures of Ag nanoparticles [22,29].

The main mechanism of the photocatalytic process is illustrated schematically in Fig. 7. The π-π conjugated bond of rGO sheet surface endows electrons with high mobility [30]. Thus it provides a good platform to transfer photo-generated protons [31] and contributes to the effective charge carrier separation during the photocatalytic process. Under light irradiation, visible-light-excitable Ag nanoparticle
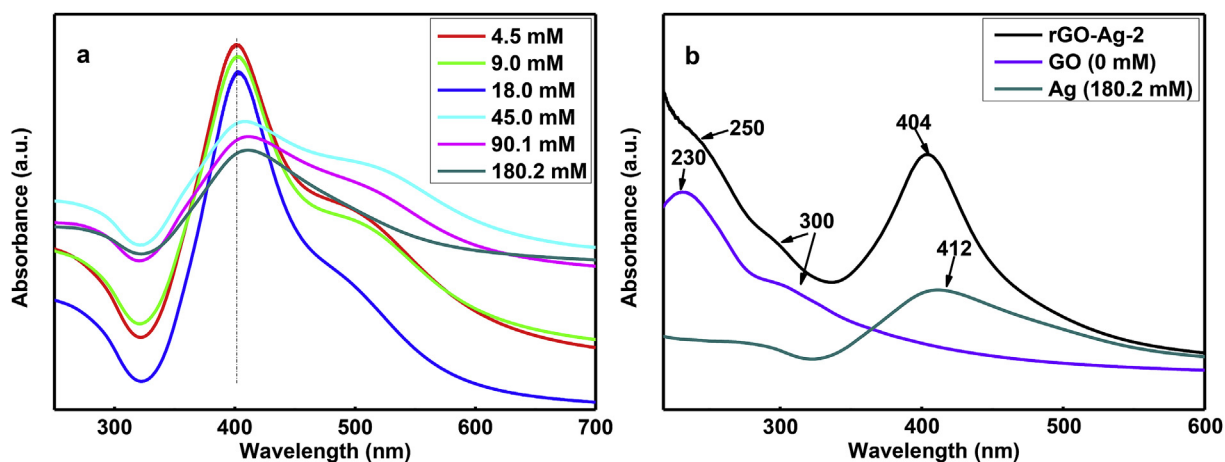
**Fig. 5.** UV–visible spectra of (a) Ag nanoparticles at different concentrations of PVP; (b) rGO-Ag-2 compared with pure Ag nanocubes and GO.
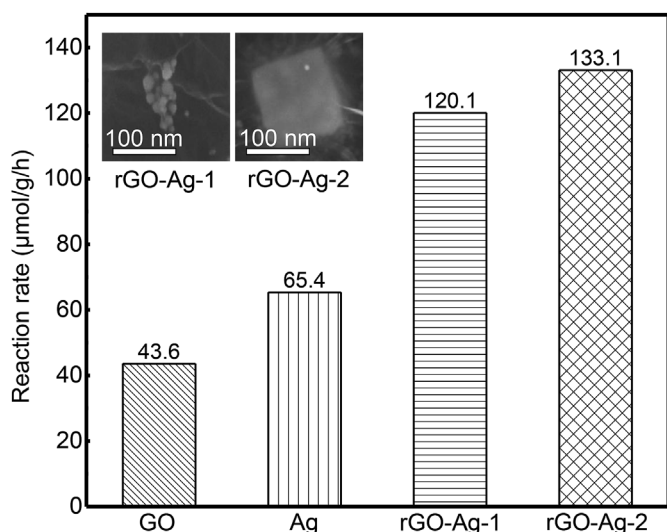


**Fig. 6.** Photocatalytic reduction of $CO_2$ by rGO-Ag-1, rGO-Ag-2, Ag nanoparticles and GO.

surface induces surface plasmon resonance [32], then the generated charge carriers (electron/hole pairs) can be spatially separated in the existence of intimately contacted rGO. Typically, electrons in high mobility can move cross the Ag/rGO interface and be injected into rGO. The well isolated electrons are valid for $CO_2$ reduction, and a higher photocatalytic activity can be obtained in Ag/rGO nanocomposite [33]. When light irradiates the metal nanoparticle surface, it induces collective oscillation for free electrons on the surface by coupling with the electromagnetic waves. If the oscillation frequency of the electrons is consistent with the frequency of the incident light, resonance appears. The resonance of electromagnetic field energy can be converted into the collective vibrational energy of free electrons, which could be restrained within the limited zone of the metallic nanoparticle surface, transforming to the local heat and then being released to the dielectric surface. The protons of Ag nanoparticle surface vibrate on its surface, generating the local heat to etch the defects of rGO sheet surface [34]. When it happens on the $sp^2$ carbon surface, protons can be highly transferred, triggering the photocatalytic $CO_2$ reduction to CO [35].

### 3.5. Mechanism of PVP directed structures of Ag nanoparticles

PVP is a well-known capping agent presenting excellent binding and coating capacities. According to the studies from Qi et al. [36,37], PVP is enabled to act as a structure-directing agent in the shape-selective synthesis of colloidal Ag nanostructures due to the preferential binding of PVP to Ag (100). During the laser ablation, plasma plume is formed in the central region of the laser ablation and the clusters rapidly coalesce to form ultrafine nanoparticles. The nitrogen atoms in the PVP molecule hinder the oxidation of $Ag^+$, and the oxygen atoms are closely adsorbed on the (100) crystal plane of Ag nanocrystals, resulting in a slow growth rate of the crystal face and thereby guiding an anisotropic crystal structure [37,38]. When the Ag substrate was irradiated by laser
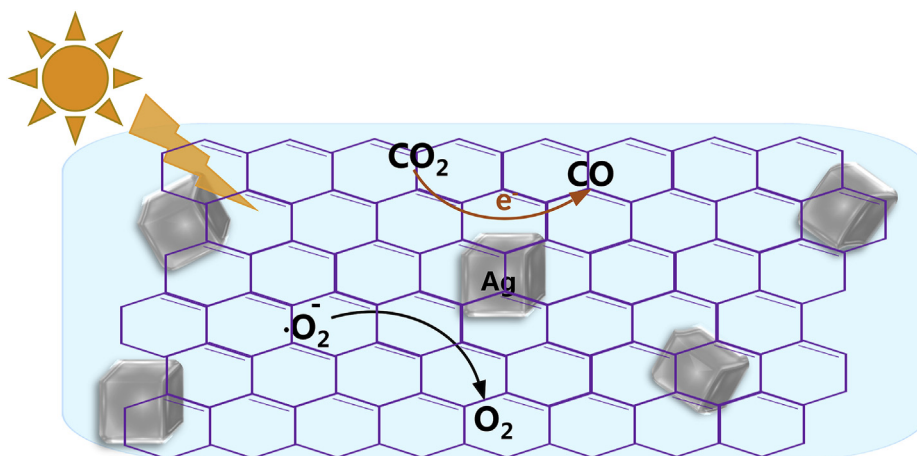


**Fig. 7.** Mechanism diagram of photocatalytic reduction of $CO_2$ by rGO-Ag-2 nanocomposites.
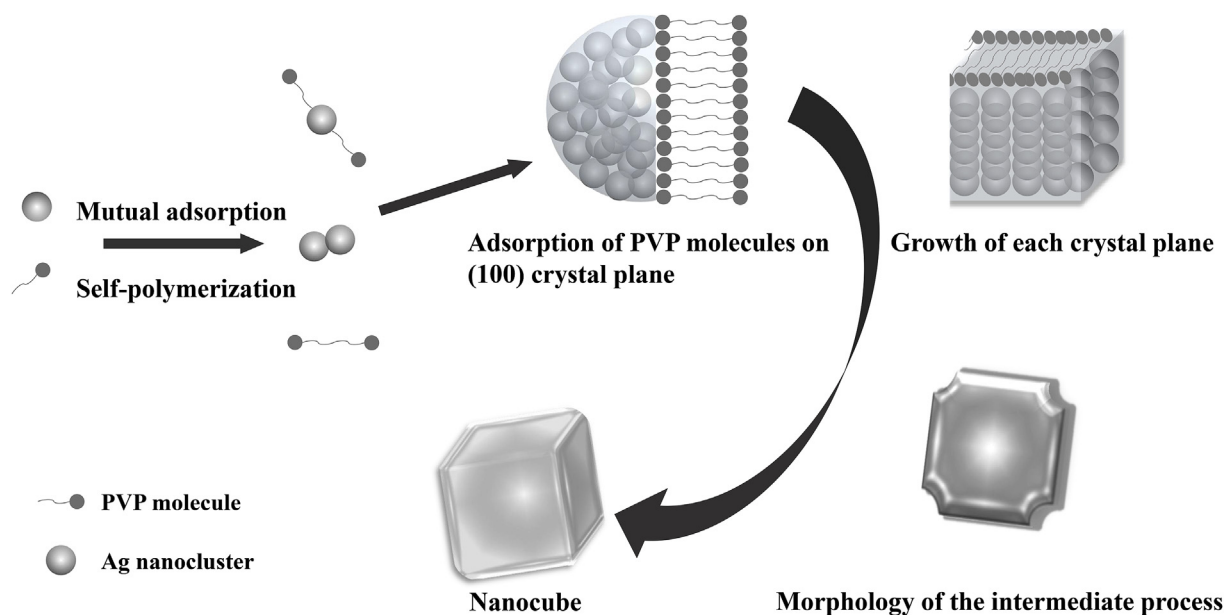
**Fig. 8.** Interaction between PVP molecules and Ag nanoparticles during the surfactant-directed formation of nanocube.

in the PVP solution, atomic bonding and cluster agglomeration can be triggered. On the other hand, the long molecular chain of PVP structure can sufficiently inhibit the particle aggregation and continuous growth. Moreover, the complexation between PVP molecules with the Ag atoms or clusters leads to the preferential absorption of PVP on the (100) crystal face of Ag, forming a characteristic face for cubic Ag nanoparticles with dominant (100) facet. When the concentration of PVP molecules becomes lower, fewer nanoclusters are adsorbed, leading to the spherical particles. By increasing the PVP concentration, Ag nanocubes gradually appear. Fig. 8 shows the schematic effect of PVP on the formation of different structures for Ag nanoparticles. While increasing the concentration of PVP, several assembly structures coexist. The concentration of PVP has a significant effect on the morphology of Ag nanoparticles. The formation of the cubic structure is attributed to the adsorption of the PVP molecules on the surface (100) of the Ag crystal. Nanoparticles are unable to grow on the surface due to the repulsive force between the active molecules, leading to the formation of cubic structure [39–41].

## 4. Conclusion

The surfactant PVP has been used to regulate the structure of Ag nanoparticles during the laser ablation in aqueous solution. The concentration of PVP significantly affects the structural morphology of Ag nanoparticles by preferable adsorption and assembly transformation. The optimized PVP concentration generates the regular polyhedral shaped Ag nanoparticles. Ag nanocube with a better dispersibility is successfully fabricated by laser ablation, which is loaded on simultaneously reduced GO support to obtain rGO-Ag nanocubes composite. The photocatalytic reduction rate of $CO_2$ could be enhanced by 2–3 times for Ag-loaded GO nanocomposite compared to individual Ag nanoparticles or graphene oxide, achieving 120.1 and 133.1 $\mu mol\, g^{-1}\, h^{-1}$ for rGO-Ag-1 (with spherical Ag nanoparticles) and rGO-Ag-2 (with Ag nanocubes), respectively. Moreover, the structural shape of Ag nanoparticles is found to present a significant impact on their photocatalytic activity, where cubic structure shows a superior activity in $CO_2$ reduction than spherical one due to the localized surface plasmon resonance coupling between the interstitial metal nanoparticles by intense local electromagnetic field generated near their sharp edges/vertices. In this case, it creates an electromagnetic hot spot to form a charge transfer complex between the Ag nanocrystal and GO

sheet, which can absorb visible light better at the excitation frequency for high-efficiency photocatalytic $CO_2$ reduction.

## Acknowledgments

## References

[1] J. Hong, W. Zhang, J. Ren, R. Xu, Anal. Methods 5 (2013) 1086–1097, https://doi.org/10.1039/c2ay26270c.

[2] N.U. Stefan, M.A. Juan Antonio, G. Hermenegildo, Anal. Methods 15 (2014) 5246–5262, https://doi.org/10.3390/ijms15045246.

[3] G.X. Chen, M.H. Hong, T.S. Ong, H.M. Lam, W.Z. Chen, H.I. Elim, Carbon 42 (2004) 2735–2737, https://doi.org/10.1016/j.carbon.2004.05.035.

[4] R. Zhou, S.D. Lin, H.X. Zong, T.T. Huang, F.P. Li, J.H. Pan, J.Q. Cui, J. Nanomater. (2017) 4604159, https://doi.org/10.1155/2017/4604159 2017.

[5] L.Q. Zhou, C. Ling, M. Jones, H. Jia, Chem. Commun. 51 (2015) 17704–17707, https://doi.org/10.1039/c5cc06752a.

[6] M.A. Asi, L. Zhu, H.E. Chun, K. Virender Sharma, D. Shu, L.I. Shuzhen, J. Yang, Y. Xiong, Catal. Today 216 (2013) 268–275, https://doi.org/10.1016/j.cattod.2013.05.021.

[7] G. Xin, C. Nie, Y. Lai, C.G. Lin, Mater. Chem. Phys. 96 (2006) 217–222, https://doi.org/10.1016/j.matchemphys.2005.07.006.

[8] B. Khodashenas, H.R. Ghorbani, Arab. J. Chem. 7 (2015), https://doi.org/10.1016/j.arabjc.2014.12.014.

[9] R. Zhou, S.D. Lin, Y. Ding, H. Yang, Y.K.K. Ong, M.H. Hong, Opto Electron. Adv. 1 (2018) 180014, https://doi.org/10.29026/oea.2018.180014.

[10] G.X. Chen, M.H. Hong, T.C. Chong, H.I. Elim, G.H. Ma, W. Ji, J. Appl. Phys. 95 (2004) 1455–1459, https://doi.org/10.1063/1.1637933.

[11] G.X. Chen, M.H. Hong, L.S. Tan, T.C. Chong, H.I. Elim, W.Z. Chen, J. Phys. Conf. Ser. 59 (2007) 289–292, https://doi.org/10.1088/1742-6596/59/1/060.

[12] A.K. Nair, K.B. Bhavitha, S. Perumbilavil, P. Sankar, D. Rouxel, M.S. Kala, S. Thomas, N. Kalarikkal, Carbon (2018) 132, https://doi.org/10.1016/j.carbon.2018.02.068 2018.

[13] J.P. Sylvestre, S. Poulin, A.V. Kabashin, M. Meunier, J.H.T. Luong, J. Phys. Chem. B 108 (2004) 16864–16869, https://doi.org/10.1021/jp047134.

[14] Y.J. Jin, L.W. Chen, M.X. Wu, X.Z. Lu, R. Zhou, M.H. Hong, Opt. Mater. Express 6 (2016) 1114–1121, https://doi.org/10.1364/OME.6.001114.

[15] M. Mahyari, A. Shaabani, Appl. Catal. Gen. 469 (2014) 524–531, https://doi.org/10.1016/j.apcata.2013.09.024.

[16] B. Jiang, Y. Wang, J.Q. Wang, C. Tian, W. Li, Q. Feng, Q. Pan, H.G. Fu, ChemCatChem 5 (2013) 1359–1367, https://doi.org/10.1002/cctc.201200684.

[17] H. Kai-Chih, Chen Dong-Hwang, Nanoscale Res. Lett. 9 (2014) 193, https://doi.org/10.1186/1556-276X-9-193.

[18] J. Low, J. Yu, W.K. Ho, J. Phys. Chem. Lett. 6 (2015) 4244–4251, https://doi.org/10.1021/acs.jpclett.5b01610.

[19] C.J. Shih, A. Vijayaraghavan, R. Krishnan, R. Sharma, J.H. Han, M.H. Ham, Z. Jin,

S. Lin, G.L. Paulus, N.F. Reuel, Q.H. Wang, D. Blankschtein, M.S. Strano, Nat. Nanotechnol. 6 (2011) 439, https://doi.org/10.1038/nnano.2011.94.

[20] A.K. Nair, K.B. Bhavitha, S. Perumbilavil, P. Sankar, D. Rouxel, M.S. Kala, S. Thomas, N. Kalarikkal, Carbon 132 (2018) 380–393, https://doi.org/10.1016/j.carbon.2018.02.068.

[21] C. Xu, X. Wang, Physicochem. Eng. Asp. 404 (2012) 78–82, https://doi.org/10.1016/j.colsurfa.2012.04.017.

[22] P. Zhang, H. Wang, X. Zhang, W. Xu, Y. Li, Q. Li, G. Wei, Z. Su, Biomater. Sci. 3 (2015) 852–860, https://doi.org/10.1039/C5BM00058K.

[23] A.R. Siekkinen, J.M. Mclellan, J.Y. Chen, Y.N. Xia, Chem. Phys. Lett. 432 (2006) 491–496, https://doi.org/10.1016/j.cplett.2006.10.095.

[24] A.R. Sadrolhosseini, A.S.M. Noor, M.A. Mahdi, A. Kharazmi, A. Zakaria, W.M.M. Yunus, N.M. Huang, IEEE Int. Conf. Photonics (2013), https://doi.org/10.1109/ICP.2013.6687068.

[25] M.J. Fernández-Merino, S. Villar-Rodil, J.I. Paredes, P. Solís-Fernández, L. Guardia, R. García, A. Martínez-Alonso, J.M.D. Tascón, Carbon 63 (2013) 30–44, https://doi.org/10.1016/j.carbon.2013.06.034.

[26] J. Li, C.Y. Liu, Eur. J. Inorg. Chem. (2010) 1244–1248, https://doi.org/10.1002/ejic.200901048 2010.

[27] T. Dreischuh, S. Gateva, A. Daskalova, A. Serafetinides, A.S. Nikolov, R.G. Nikov, N.N. Nedyalkov, P.A. Atanasov, M.T. Alexandrov, D.B. Karashanova, N.E. Marinkov, I.Z. Dimitrov, I.I. Boevski, A. Visan, I.N. Mihailescu, Int. Soc. Opt. Photonics (2017) 102260C, https://doi.org/10.1117/12.2262450.

[28] A.S. Nikolov, N.N. Nedyalkov, R.G. Nikov, P.A. Atanasov, M.T. Alexandrov, D.B. Karashanova, Appl. Phys. A 109 (2012) 315–322, https://doi.org/10.1007/s00339-012-7094-0.

[29] J. Rosen, G.S. Hutchings, Q. Lu, S. Rivera, Y. Zhou, D.G. Vlachos, F. Jiao, ACS Catal. 5 (2015), https://doi.org/10.1021/acscatal.5b00840 150605133022004.

[30] C.Y. Zhang, R. Hao, B. Zhao, Y. Fu, H. Zhang, S. Moeendarbari, C.S. Pickering, Y.W. Hao, Y.Q. Liu, Appl. Surf. Sci. 400 (2016) 49–56, https://doi.org/10.1016/j.apsusc.2016.12.161.

[31] A.H. Castro Neto, F. Guinea, N.M.R. Peres, K.S. Novoselov, A.K. Geim, Rev. Mod. Phys. 81 (2009) 109–162, https://doi.org/10.1103/RevModPhys.81.109.

[32] S.K. Bhunia, N.R. Jana, ACS Appl. Mater. Interfaces 6 (2014) 20085–20092, https://doi.org/10.1021/am505677x.

[33] C.H. Liu, M.H. Hong, Y. Zhou, G.X. Chen, M.M. Saw, A.T.S. Hor, Phys. Scr. T129 (2007) 326–328, https://doi.org/10.1088/0031-8949/2007/T129/072.

[34] H. Zong, T. Zhao, G. Zhou, R. Qian, T. Feng, J.H. Pan, Catal. Today 335 (2019) 252–261, https://doi.org/10.1016/j.cattod.2018.12.015.

[35] L. Deng, H. Guo, J. Cui, X. Chen, L.J.M.L. Miao, Mater. Lett. 197 (2017) 45–47, https://doi.org/10.1016/j.matlet.2017.03.153.

[36] S. Zhong, W. Jiang, M. Han, G.Z. Liu, N. Zhang, Y. Lu, Appl. Surf. Sci. 347 (2015) 242–249, https://doi.org/10.1016/j.apsusc.2015.04.080.

[37] X. Qi, T. Balankura, Y. Zhou, K.A.J.N.L. Fichthorn, Nano Lett. 15 (2015) 7711, https://doi.org/10.1021/acs.nanolett.5b04204.

[38] K.M. Koczkur, S. Mourdikoudis, L. Polavarapu, S.E. Skrabalak, Dalton Trans. 44 (2015) 17883–17905, https://doi.org/10.1039/C5DT02964C.

[39] X. Jiang, M. Manawan, T. Feng, R. Qian, T. Zhao, G. Zhou, F. Kong, Q. Wang, S. Dai, J.H. Pan, Catal. Today 300 (2018) 12–17, https://doi.org/10.1016/j.cattod.2017.06.010.

[40] R. Qian, H. Zong, J. Schneider, G. Zhou, T. Zhao, Y. Li, J. Yang, D.W. Bahnemann, J.H. Pan, Catal. Today 335 (2019) 78–90, https://doi.org/10.1016/j.cattod.2018.10.053.

[41] G. Zhou, T. Zhao, R. Qian, X. Xia, S. Dai, A. Alsaedi, T. Hayat, J.H. Pan, Catal. Today 335 (2019) 365–371, https://doi.org/10.1016/j.cattod.2018.12.004.